



First-principles and experimental investigations on ductility/brittleness of intermetallic compounds and joint properties in steel/aluminum laser welding

Tian LI¹, Dian-wu ZHOU¹, You-rui-ling YAN¹, Ping PENG², Jin-shui LIU²

1. State Key Laboratory of Advanced Design and Manufacturing for Vehicle Body,
Hunan University, Changsha 410082, China;

2. School of Materials Science and Engineering, Hunan University, Changsha 410082, China

Received 18 September 2020; accepted 28 June 2021

Abstract: Morphology, distribution, composition, forming ability, structural stability and intrinsic mechanical properties of the intermetallic compounds (IMCs) formed in steel/aluminum laser welding were determined through scanning electron microscope, energy dispersive spectrometer, X-ray diffractometer and first-principles calculation. It was found that the mechanical properties of the joint are limited by the Fe–Al IMCs, whose brittleness is attributed to the orbital hybridization between Al(s), Al(p) and Fe(d). However, the joint properties are improved by adding interlayer, which is ascribed to some changes of electronic structure of the generated IMCs. The transition mechanism of IMCs changing from brittle to ductile is mainly due to the weak ability of interlayer elements to attract electrons. The mechanical properties of the joint are closely related to the ductility or brittleness of the IMCs. Moreover, the addition of Ti foil interlayer effectively improves the mechanical properties of the joints, which means that the experimental verification is in good agreement with the theoretical calculation predictions.

Key words: first-principles calculation; elastic constant; ductility; brittleness; laser welding; mechanical properties

1 Introduction

As the energy crisis and the greenhouse effect become more and more serious, problems such as energy conservation and emission reduction need be solved urgently in all countries of the world [1–3]. The introduction of the lightweight concept in automotive industry has greatly alleviated the pressure of this situation. Light weighting can be achieved by replacing part of steels with aluminum alloys on the body, which means that it is inevitable for the steel/aluminum hybrid structure [4].

For metallic materials, many scholars are trying to establish the connection between the microscopic intrinsic mechanical properties and the

macroscopic mechanical properties. PUGH [5] proposed a model to predict the brittle/ductile behavior of materials by the ratio of the bulk modulus (B) and shear modulus (G), in which the values of B and G respectively reflect the resistance to fracture and plastic deformation. GANESHAN et al [6] characterized and judged the brittleness of IMCs by the use of elastic moduli such as B and G . SHINODA et al [7] believed that the elastic constant can be used to characterize the mechanical strength of solid materials. SUMER and SMITH [8] thought that the elastic constant and elastic modulus can be used to evaluate the mechanical properties of the material, and they believed that the smaller the difference between the elastic constant and elastic modulus is, the better the shaping ability of the

material is. MATTESINI et al [9] introduced that the Poisson's ratio could characterize the elastic properties of materials by quantifying the shear resistance stability of crystals, and they thought that the larger the Poisson's ratio is, the better the structural shaping ability of the corresponding material will be. GSCHNEIDNER et al [10] hold that a certain critical value of Poisson's ratio could determine the ductility or brittleness of the *B2*-structured IMCs, where they would be brittle when the Poisson's ratio exceeds the critical value, otherwise they are ductile. In addition, the elastic anisotropy of the crystal is closely related to the possibility of inducing micro-cracks in material, which is of great significance in engineering science [11]. LIU and COHEN [12] showed that the hardness and shear modulus of the material have a strong correlation. Based on the above research, it could be found that the microscopic property of the material has close relationship with the macroscopic mechanical property.

Laser welding has been widely used in the welding of heterogeneous metal materials due to its advantages of high energy density, narrow heat-affected zone, low deformation, and easy automation [13]. As far as steel/aluminum laser welding was concerned, it was found that the mechanical properties of the joint can be effectively improved through metallurgical control, such as adding Ni foil [14] and Sn powder [15], and some new IMCs such as $\text{Ni}_{1.1}\text{Al}_{0.9}$ and FeSn were formed with the addition of alloying elements. Thus, it could be speculated that the improvement of joint mechanical properties was related to its intrinsic mechanical properties.

In previous work [15–18], first-principles calculation was applied in studying laser welding. In this work, we further extended the application of alloying method in steel/aluminum laser welding. Firstly, the thermodynamics and intrinsic mechanical properties were calculated for the generated IMCs from Refs. [14,15,19], the key factor in limiting the joint mechanical properties was determined, and how to improve the joint performance was speculated. Secondly, the alloying element which is beneficial to improving the steel/aluminum joint properties, was proposed. Finally, laser welding experiment and SEM, EDS, XRD, shear–tensile test technologies were conducted for verification. The electronic structural

root of brittle phase and the mechanism of IMCs transforming from brittle to ductile were analyzed and discussed. Through the research, the project results will provide a new perspective to the steel/aluminum dissimilar material laser welding, and also provide a theoretical basis for alloying metallurgical control of dissimilar material welding.

2 Calculation conditions, materials and experimental procedure

The Cambridge Serial Total Energy Package (CASTEP) [20] was used to calculate heats of formation and elastic constants of the generated IMCs in the steel/aluminum laser welding. CASTEP adopts plane wave pseudopotential to fulfill first principles quantum mechanics calculations, which is based on density functional theory (DFT). In this calculation method, the total energy includes kinetic energy, electrostatic energy, and exchange correlation energy. The exchange correlation energy could be calculated in the form of Perdew–Burke–Ernzerhof (PBE) in generalized gradient approximation (GGA) [21] on a minimized fast Fourier transform (FFT) grid, the ultrasoft [22] pseudopotential which relaxed the regular condition was used as the plane wave base set, the calculation was performed using a self-consistent iterative method, and the electronic relaxation was processed using a Pulay density hybrid scheme combining the Broyden–Fletcher–Goldfarb–Shanno (BFGS) [23] conjugate gradient method. In addition, the cutoff energy of atomic wave functions was set at 330 eV when performing single point energy calculation. In order to define the real space grid, a standard Monkhorst–Pack $6\times 6\times 6$ *k*-point grid was selected. When the unit cell structure has been optimized, the convergence value of the total energy of the system was set as 5.0×10^{-6} eV/atom, the force on each atom was less than 0.1 eV/nm, the tolerance offset was less than 5.0×10^{-5} nm, and the stress deviation was less than 0.02 GPa. When calculating the elastic constants of phases, the PW91 form was adopted for computing the exchange correlation energy in GGA. The dynamics module of DMol program was used to calculate the thermodynamic properties at different temperatures, such as Gibbs free energy and heat capacity. During the calculation, the canonical ensemble (NVT) was selected for macro ensemble, the Becke–Lee–

Yang–Parr (BLYP) was adopted as the electron exchange correlation energy [24] in GGA, the full electron potential was taken as the potential function, and the double numerical basis function (DNP) with d orbit was chosen as the electronic wave function. The fine grid scatter and smearing energy were used for fast energy convergence.

In this study, a 4 kW fiber laser was used to weld 1.4 mm-thick DP590 dual-phase steel and 1.5 mm-thick 6022 aluminum alloy in an overlap steel-on-aluminum configuration due to the high reflection of aluminum. The welding schematic is shown in Fig. 1. The chemical composition of DP590 dual-phase steel and 6022 aluminum alloy was 2.5Mn–0.6Si–0.15C (wt.%), 0.85Si–0.55Mg–0.25Fe (wt.%), respectively. Ti was selected as the alloying element. It was added in the form of foil to ensure the uniformity, and the thickness was 0.01 mm. The main process parameters of the laser welding were determined based on the acceptable weld formability as listed in Table 1.

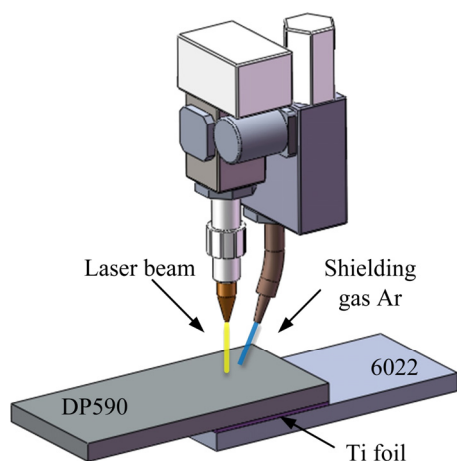


Fig. 1 Schematic illustration of laser welding arrangement

Table 1 Welding parameters used in present work

Parameter	Value
Laser power/W	1600
Laser defocus/mm	0
Welding speed/(mm·s ⁻¹)	30
Flow rate of Ar gas/(L·min ⁻¹)	10

After welding, standard metallographic specimens were prepared and etched with nital etchant (4% HNO₃ + 96% C₂H₅OH). The micro-morphology of the interface and fracture morphology of each joint were observed through

scanning electron microscopy (SEM), the interfacial phase composition of the molten pool was determined by energy dispersive X-ray spectroscopy (EDS) and confirmed by X-ray diffraction (XRD). The standard shear–tensile samples were made based on the GB/T 228.1–2010 standard and measured on the 3369-type electronic universal testing machine with a rate of 0.1 mm/min at the room temperature. The dimensional drawing of the specimens and the schematic diagram of the shear–tensile test are shown in Fig. 2. The mechanical property of the joint was characterized by the maximum load, which was the average value of at least three specimens to ensure the accuracy of the experiment.

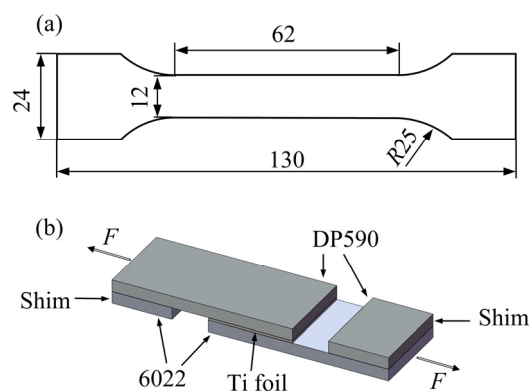


Fig. 2 Dimensional drawing (a) and schematic diagram (b) of shear–tensile experiment (unit: mm)

3 First-principles calculation and discussion

In order to reveal the formation mechanism of the IMCs and the improvement of the joint properties with the addition of interlayer Sn and Ni, the intrinsic mechanical properties, such as heats of formation, elastic constant, Gibbs free energy, density of state and electron density difference of the phases, were calculated and analyzed. Researchers have shown that Fe₂Al₅, Fe₂Ti and TiAl₃ are easily formed in the metallurgical reaction of Fe–Al, Fe–Ti and Ti–Al binary systems [25–27]. Besides, the experiment results indicated that the IMCs, such as FeSn, FeAl, FeAl₃, Ni_{1.1}Al_{0.9} and FeAl₃, were generated after adding Sn powder and Ni foil. In addition, NiAl can approximately replace Ni_{1.1}Al_{0.9} in the view of the fact that Ni_{1.1}Al_{0.9} is a non-equilibrium phase and the crystal structure is similar to NiAl. Therefore, the intrinsic mechanical properties of FeAl, Fe₂Al₅, FeAl₃, FeSn, NiAl,

Fe_2Ti and TiAl_3 phases would be calculated in the following part.

3.1 Crystal structures and heats of formation

The unit cell structures of FeAl , Fe_2Al_5 , FeAl_3 , FeSn , NiAl , Fe_2Ti and TiAl_3 phases are displayed in Fig. 3. The equilibrium lattice constants of each phase are tabulated in Table 2. As shown in Table 2, the calculated lattice constants of each phase in the present work exhibit a good agreement with other calculated [28–36] and experimental values [37–41]. Hence, the selection of each unit cell model in this work is suitable.

Heats of formation (ΔH) of each phase formed during the process of welding were calculated

according to the following equation [43]:

$$\Delta H = E_{\text{tot}}^{\text{AB}} - [cE_{\text{solid}}^{\text{A}} + (1-c)E_{\text{solid}}^{\text{B}}] \quad (1)$$

where $E_{\text{tot}}^{\text{AB}}$ refers to the total energy of each atom of the IMCs, $E_{\text{solid}}^{\text{A}}$ and $E_{\text{solid}}^{\text{B}}$ represent the energy of each atom of the solid elements A and B, respectively, and c is the mass fraction of component A. The energies of the solid atom were calculated through utilizing the same code as crystal model, then the value of $E_{\text{tot}}^{\text{AB}}$ could be obtained through dividing the energy of the unit cell by the number of atoms involved in the crystal. The calculated solid atomic energies of Fe, Al, Sn, Ni and Ti in this work are -864.673 , -56.404 , -95.456 , -1354.31 and -1603.062 eV, respectively. By using

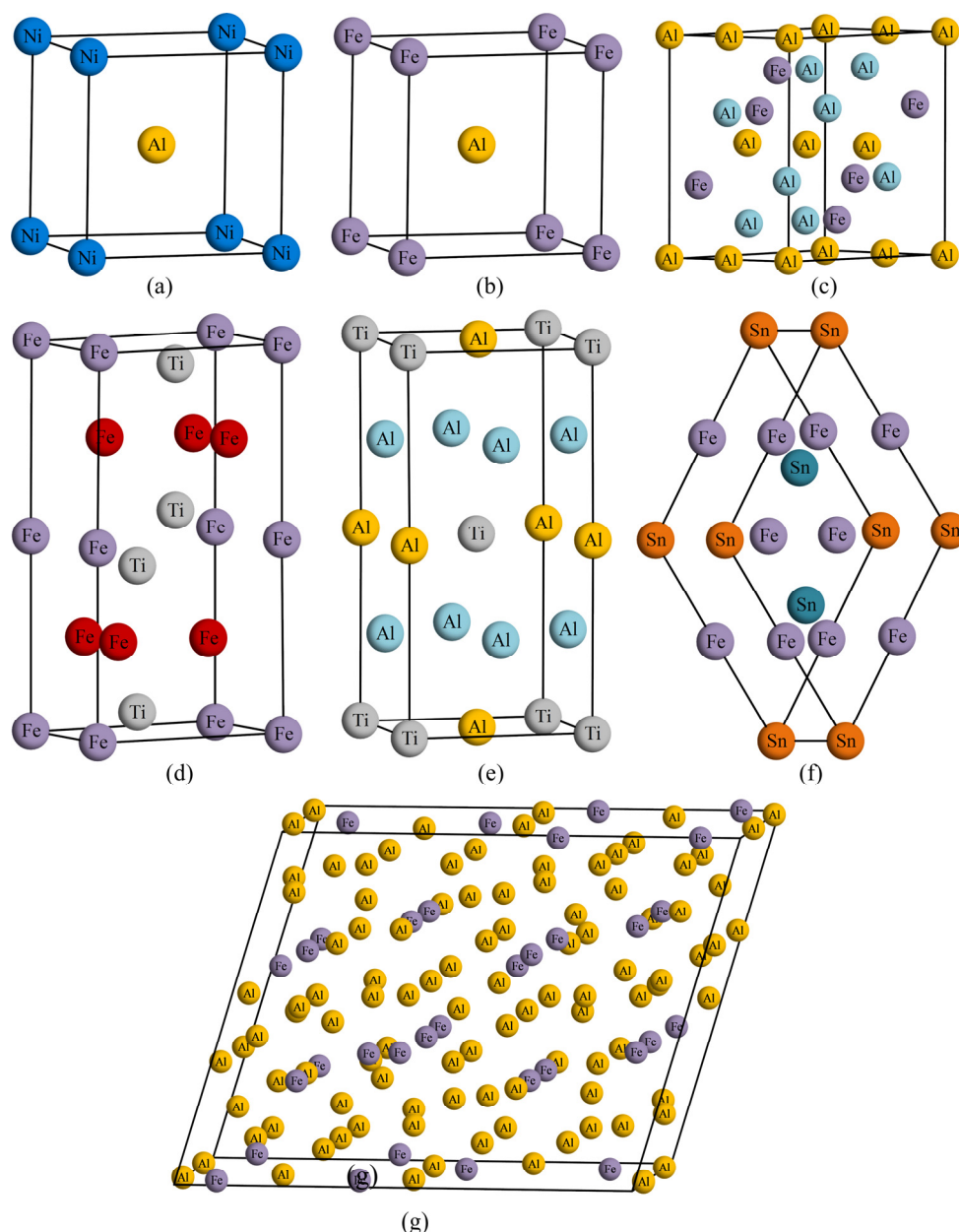


Fig. 3 Crystal structures of NiAl (a), FeAl (b), Fe_2Al_5 (c), Fe_2Ti (d), TiAl_3 (e), FeSn (f) and FeAl_3 (g) phases

Table 2 Lattice constants of FeAl, Fe₂Al₅, FeAl₃, FeSn, NiAl, Fe₂Ti and TiAl₃ phases

Phase	Present			Ref.			Exp.		
	<i>a</i> /Å	<i>b</i> /Å	<i>c</i> /Å	<i>a</i> /Å	<i>b</i> /Å	<i>c</i> /Å	<i>a</i> /Å	<i>b</i> /Å	<i>c</i> /Å
FeAl	2.908	2.908	2.908	2.900 ^a	2.900 ^a	2.900 ^a	2.910 ^j	2.910 ^j	2.910 ^j
				2.919 ^b	2.919 ^b	2.919 ^b	2.920 ^k	2.920 ^k	2.920 ^k
				2.86 ^c	2.86 ^c	2.86 ^c	2.909 ^l	2.909 ^l	2.909 ^l
Fe ₂ Al ₅	7.675	6.403	4.203	7.622 ^d	6.323 ^d	4.178 ^d	–	–	–
FeAl ₃	15.489	8.083	12.476	–	–	–	–	–	–
FeSn	5.307	5.307	4.445	–	–	–	–	–	–
NiAl	2.848	2.848	2.848	2.84 ^e	2.84 ^e	2.84 ^e	2.89 ^m	2.89 ^m	2.89 ^m
				2.82 ^f	2.82 ^f	2.82 ^f	2.88 ⁿ	2.88 ⁿ	2.88 ⁿ
Fe ₂ Ti	4.790	4.790	7.810	4.666 ^g	4.666 ^g	7.772 ^g	4.796 ^o	4.796 ^o	4.796 ^o
TiAl ₃	3.854	3.854	3.854	3.845 ^h	3.845 ^h	8.609 ^h	3.840 ^p	3.840 ^p	8.579 ^p
				3.78 ⁱ	3.78 ⁱ	8.51 ⁱ	3.78 ^q	3.78 ^q	8.51 ^q

^a Ref. [28]; ^b Ref. [29]; ^c Ref. [30]; ^d Ref. [31]; ^e Ref. [32], LAPW LDA; ^f Ref. [33], FLAPW LDA; ^g Ref. [34]; ^h Ref. [35]; ⁱ Ref. [36]; ^j Ref. [37]; ^k Ref. [38]; ^l Ref. [39]; ^m Ref. [37]; ⁿ Ref. [42]; ^o Ref. [40]; ^p Ref. [41]; ^q Ref. [41]

the optimized compounds total energies, the values of ΔH of the phases were obtained and shown in Table 3.

According to Table 3, heats of formation of FeAl, NiAl and TiAl₃ are -64.65 , -69.57 and -43.03 kJ/mol, which are highly consistent with the other calculations [36,44–47] and experiment results [48–54]. The slight difference may be caused by different calculation methods such as full-potential-linear-muffin-tin-orbital (FP-LMTO), full-potential linearized augmented plane-wave (FLAPW) LDF, and calorimetric. Hence, the calculation conditions and parameters chosen in this paper are suitable, and the calculation results of Fe₂Al₅, FeAl₃, FeSn and Fe₂Ti are credible. We can further conclude that all the IMCs can be formed due to their values of heats of formation being negative, which verifies the experimental results.

3.2 Elastic properties and hardness

This part will discuss the elastic properties of the above-mentioned IMCs and investigate how the alloying elements influence the joint mechanical properties. The elastic constant C_{ij} is a physical quantity which characterizes the resistance of crystal in solid material to external stress, and it is of great significance for the mechanical properties of the material [55]. Based on the value of elastic constant, the information of bonding property,

Table 3 Heats of formation of FeAl, Fe₂Al₅, FeAl₃, FeSn, NiAl, Fe₂Ti and TiAl₃ phases

Phase	Heat of formation/(kJ·mol ⁻¹)		
	Present	Ref.	Exp.
FeAl	-64.65	-51.14 ^a	-47.28 ^f , -59.82 ^g
Fe ₂ Al ₅	-25.10	–	–
FeAl ₃	-28.17	–	–
FeSn	-13.22	–	–
NiAl	-69.57	-64.74 ^b	–
Fe ₂ Ti	-66.48	–	–
TiAl ₃	-43.03	-41.49 ^c , -41.49 ^d	-38 ^h , -38.6 ⁱ , -39 ^j ,
		-40.52 ^e	-35.6 ^k , -36.6 ^l

^a Ref. [44], DFT PAW GGA; ^b Ref. [45] DFT; ^c Ref. [46], FP-LMTO; ^d Ref. [36], FLAPW LDF; ^e Ref. [47], LMTO ASA; ^f Ref. [48], calorimetric; ^g Ref. [49]; ^h Ref. [50], calorimetric; ⁱ Ref. [51], DSC; ^j Ref. [52], calorimetric; ^k Ref. [53], calorimetric; ^l Ref. [54], calorimetric

bonding anisotropy and structural stability between adjacent atomic planes will be obtained. Therefore, the mechanical stability of unstressed crystal structures can be deduced from the elastic constant. The elastic constants and the relevant moduli of each phase above are shown in Table 4.

The mechanical stability of the crystal structure is determined by the elastic constant, and different crystal systems correspond to different mechanical stability conditions. In this work, FeSn

Table 4 Elastic constants and moduli of FeAl, Fe₂Al₅, FeSn, NiAl, Fe₂Ti and TiAl₃ phases

Phase	Source	Elastic constant/GPa			Modulus/GPa			<i>G/B</i>	ν
		<i>C</i> ₁₁	<i>C</i> ₁₂	<i>C</i> ₄₄	<i>B</i>	<i>G</i>	<i>E</i>		
FeAl	Present	207.57	100.26	122.35	136.03	94.87	230.93	0.7	0.22
	Cal.	183.3 ^a	107.0 ^a	107.0 ^a	156 ^a	–	–	–	–
	Cal.	192.24 ^b	120.15 ^b	116.95 ^b	124.6 ^c	–	–	–	–
	Exp.	207.7 ^d	121.4 ^d	126.2 ^d	–	–	–	–	–
	Exp.	181.1 ^e	113.7 ^e	127.1 ^e	136.1 ^e	–	–	–	–
Fe ₂ Al ₅	Present	234.65	45.59	84.17	108.61	88.32	208.45	0.81	0.18
FeSn	Present	187.68	121.166	61.43	143.34	50.163	134.76	0.35	0.34
NiAl	Present	204.14	184.706	120.45	191.18	76.158	201.69	0.40	0.32
	Cal.	262 ^f	146 ^f	138 ^f	185 ^f	–	–	–	–
	Cal.	236 ^g	167 ^g	140 ^g	187 ^g	–	–	–	–
	Exp.	212 ^h	143 ^h	112 ^h	166 ^h	70 ^h	184 ^h	0.42 ^h	–
	Exp.	205 ⁱ	135 ⁱ	117 ⁱ	–	–	–	–	–
Fe ₂ Ti	Present	270.26	113.15	67.45	165.53	71.89	188.40	0.43	0.31
TiAl ₃	Present	181.98	88.58	89.90	119.71	72.62	181.21	0.61	0.25
	Cal.	202 ^j	88 ^j	20 ^j	118 ^j	68 ^j	170 ^j	0.58 ^j	0.25 ^j
	Exp.	217.7 ^k	57.7 ^k	92.0 ^k	105.6 ^k	93.0 ^k	215.7 ^k	0.88 ^k	0.16 ^k

^a Ref. [28], tight-binding linear-muffin-tin-orbital (TB-LMTO); ^b Ref. [57], embedded atom method (EAM); ^c Ref. [29], modified embedded-atom method (MEAM); ^d Ref. [30], DFT GGA; ^e Ref. [39]; ^f Ref. [32], LAPW LDA; ^g Ref. [33], FLAPW LDA; ^h Ref. [58]; ⁱ Ref. [59], expt., ultrasonic pulse-echo method at 295 K; ^j Ref. [36], FLAPWLDF; ^k Ref. [60], expt., the velocity of ultrasonic waves

and Fe₂Ti belong to the hexagonal crystal system, NiAl and FeAl belong to the cubic crystal system, while TiAl₃ and Fe₂Al₅ belong to the tetragonal and orthorhombic crystal systems, respectively. According to the report in Ref. [56], in terms of hexagonal and tetragonal systems, the corresponding conditions are as follows:

$$C_{11} > |C_{12}|, C_{33}(C_{11} + C_{12}) > 2C_{13}^2, C_{44} > 0, C_{66} > 0 \quad (2)$$

While in the case of cubic crystal system, *C*₁₁, *C*₁₂ and *C*₄₄ are three independent elastic constants and the completely necessary and sufficient Born stability criteria are well known:

$$C_{11} - C_{12} > 0, C_{11} + 2C_{12} > 0, C_{44} > 0 \quad (3)$$

For orthorhombic crystal system, the mechanical stability of the structure requires the constants satisfying the following conditions:

$$C_{ii} > 0, C_{ii} + C_{jj} - 2C_{ij} > 0, C_{11} + C_{22} + C_{33} + 2(C_{12} + C_{13} + C_{23}) > 0 \quad (4)$$

According to the results of elastic constants *C*_{*ij*} (GPa) in Table 4, all the above criteria are easily satisfied by the phases in this work, which means

that all these binary phases are mechanically stable. The available data of FeAl, NiAl and TiAl₃ phases obtained from other articles [28,32,33,36,57] and experimental results [30,39,58–60] are simultaneously summarized in Table 4, with which the current results share good consistence, indicating the suitability of the elastic constant calculation conditions selected in this work. According to the current research status, there is no relevant report on the elastic constant data of Fe₂Al₅, FeSn and Fe₂Ti. Since the calculated data in this work conform to the generalized criteria for the thermo-elastic stability of hexagon and quadrilateral class (Eq. (2)), the calculation results of the elastic constants of Fe₂Al₅, FeSn and Fe₂Ti are credible.

Furthermore, the bulk modulus *B*, shear modulus *G*, elastic modulus *E* and Poisson's ratio (ν) can be derived from the following equations [61]:

$$B = \frac{C_{11} + 2C_{12}}{3} \quad (5)$$

$$G = \frac{1}{5}(C_{11} - C_{12} + 3C_{44}) \quad (6)$$

$$E = \frac{(C_{11} - C_{12} + 3C_{44})(C_{11} + 2C_{12})}{2C_{11} + 3C_{12} + C_{44}} \quad (7)$$

$$\nu = \frac{3B - E}{6B} \quad (8)$$

Based on the above formulas, the mechanical parameters of each compound are also tabulated in Table 4. From Table 4, for the bulk modulus B of FeAl, there is a slight deviation between the present calculation results and existing calculation data [28,29], which may be caused by various calculation methods. But they are well consistent with the experimental values [39]. Similarly, the calculation result of B of NiAl is highly consistent with the values in Refs. [32,33], and the moduli values are very close to the experimental results [58]. In the case of TiAl₃, the results indicate that the values of each modulus and Poisson's ratio in the present work agree well with previous calculations with FLAPW method [36]. In addition, the deviation between the calculated value and the experimental value [60] is within the acceptable range. Thus, the values of various moduli and Poisson's ratios calculated by the elastic constants in this paper are reliable. Studies have shown that Poisson's ratio (ν) is commonly used to evaluate the structural stability of crystals against shear, the larger the value is, the better the plasticity of the structure is [9]. According to Table 4, the plasticity of each phase from strong to weak follows the order of FeSn, NiAl, Fe₂Ti, TiAl₃, FeAl and Fe₂Al₅. Besides, elastic modulus (E) is also an important parameter for judging the material plasticity [8]. In contrast to Poisson's ratio (ν), the smaller the E value is, the better the plasticity of the structure is. It can be seen from Table 4 that, the plasticity reduces in the order of FeSn, TiAl₃, Fe₂Ti, NiAl, Fe₂Al₅ and FeAl. Although the orders of the plasticity deduced from ν and E are different, the plasticities of new phases after adding alloying elements such as FeSn, NiAl, Fe₂Ti and TiAl₃ are all stronger than that of the Fe–Al phases. Therefore, adding alloying elements could improve the plasticity of the steel and aluminum welding joint.

More importantly, there are several criteria to judge the material's brittleness or ductility by elastic constants. Firstly, PUGH [5] proposed that the G/B ratio could be used to determine the material's ductility or brittleness. When the ratio is

less than 0.5, it is a tough phase, otherwise it is a brittle one. Therefore, FeSn, NiAl and Fe₂Ti are ductile phases and the others are brittle phases. Secondly, the Cauchy pressure parameters C_{12} – C_{44} can also be used to predict the ductility (brittleness) of materials. The positive or negative of Cauchy pressure parameter value can estimate whether the atoms in the structure are bonded by metallic bonds or covalent bonds. When the value is positive there is a metallic bond and the material performs the ductile behavior. Otherwise, the bonding type is covalent and the material is brittle [62]. According to Table 4, we can easily observe that the Cauchy pressure parameter values of FeSn, NiAl and Fe₂Ti are positive and the others are negative. Thus, it can be deduced that FeSn, NiAl and Fe₂Ti are ductile phases and FeAl, Fe₂Al₅, TiAl₃ are brittle phases, which is consistent well with the conclusion of the first criterion.

Furthermore, studies have shown that the hardness of a material is the intrinsic resistance to deformation [63]. CHEN et al [64] proposed Eq. (9) that G/B can not only characterize the ductility or brittleness of the material, but also be correlated with the hardness of the material (H_V).

$$H_V = 2(k^2G)^{0.585} - 3 \quad (9)$$

where k refers to the ratio of shear modulus to bulk modulus G/B . Therefore, the Vickers hardness results of FeAl, Fe₂Al₅, FeSn, NiAl, Fe₂Ti and TiAl₃ phases are 15.9, 18.5, 2.79, 5.64, 6.09 and 10.76 GPa, respectively. Namely, the Vickers hardness values of the above phases gradually decrease in the order of Fe₂Al₅, FeAl, TiAl₃, Fe₂Ti, NiAl and FeSn, which is completely consistent with the order that the G/B value of each phase gradually decreases. Generally, the higher the hardness of the material is, the greater the brittleness is. Therefore, the hardness calculation results further prove the reliability of the calculation results of each phase's ductility or brittleness.

According to the calculation results of the elastic constants and hardness, the high-plasticity ductile IMCs were formed after adding alloying elements of Sn and Ni, and the corresponding experimental results showed that the mechanical properties of the joints have been significantly improved. Therefore, we can say that the generation of ductile phase is the main reason for the improvement of the joint performance. In addition,

the new formed phases of Fe_2Ti and TiAl_3 refer to the ductile and low-brittleness phases respectively with the addition of Ti alloying element, which that means the mechanical properties of the joint will be also enhanced.

3.3 Transformation mechanism of IMCs from brittle to ductile

To reveal the IMCs transforming from brittle to ductile after adding alloying elements, firstly, total and partial densities of states (DOS) were used to investigate the bonding of FeSn, Fe_2Ti and FeAl phases. According to Figs. 4(a–c), the electron energy of all phases that contribute to bonding is mainly concentrated in the range of -10 to 0 eV,

and the bonding peaks mainly originate from the contribution of valence electron numbers of Fe(d), Sn(s) and Sn(p) orbits for FeSn (as shown in Fig. 4(a)). From Fig. 4(b), the main bonding peaks of Fe_2Ti mainly derived from the contribution of valence electron numbers of Fe(d), Ti(p) and Ti(d). Similarly, in the case of FeAl, the main bonding peaks mostly result from the hybridization of Fe(d), Al(s) and Al(p) orbits, respectively. Further analysis shows that there is a wide bond gap at the Fermi level of Al(s), which is an obvious covalent bond characteristic. This strong covalent bond feature is the root of the electronic structure of the brittle phase.

Secondly, Fig. 5 shows the differential charge

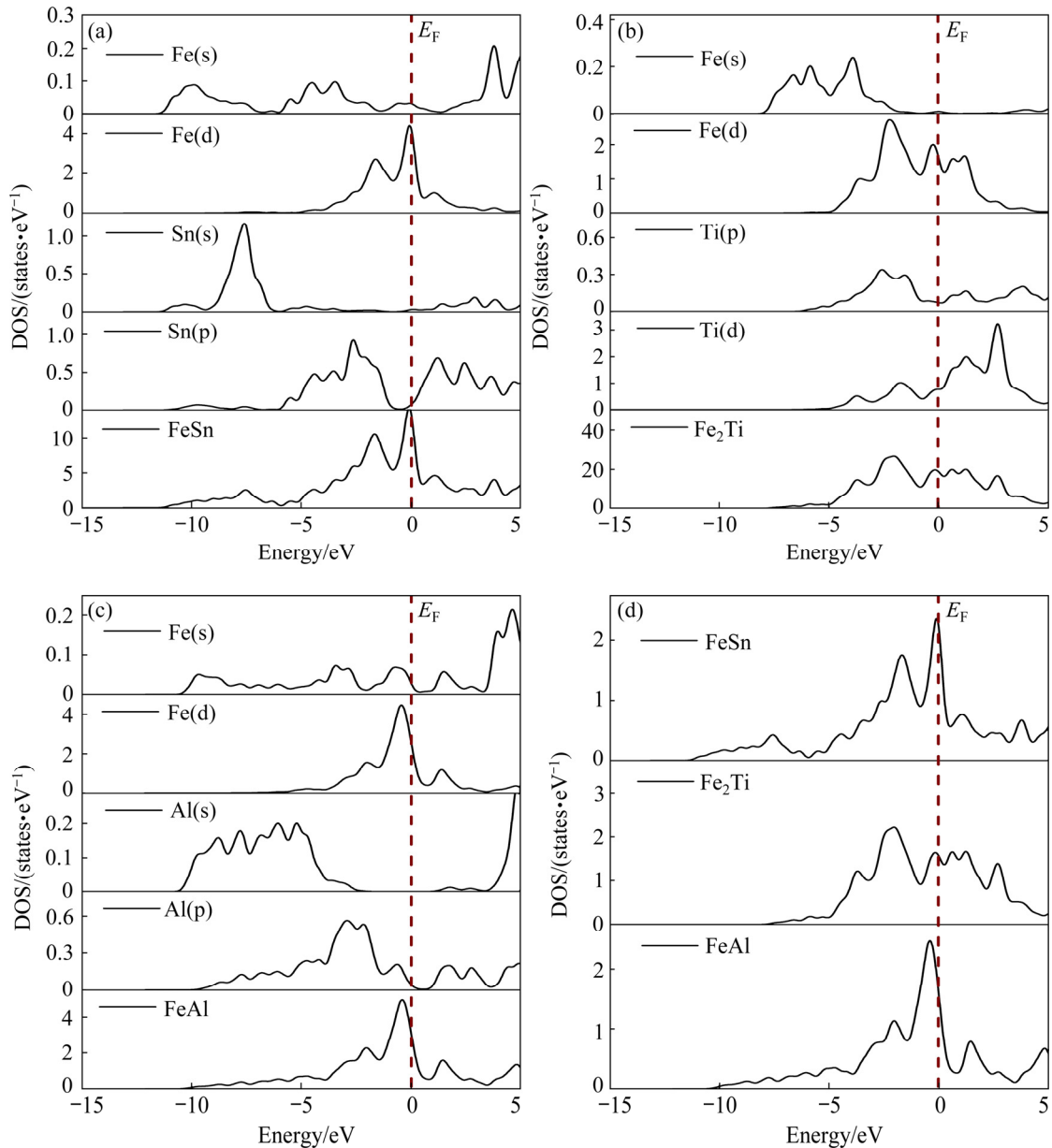


Fig. 4 DOS of FeSn (a), Fe_2Ti (b), FeAl (c), FeSn, Fe_2Ti and FeAl (d) per atom

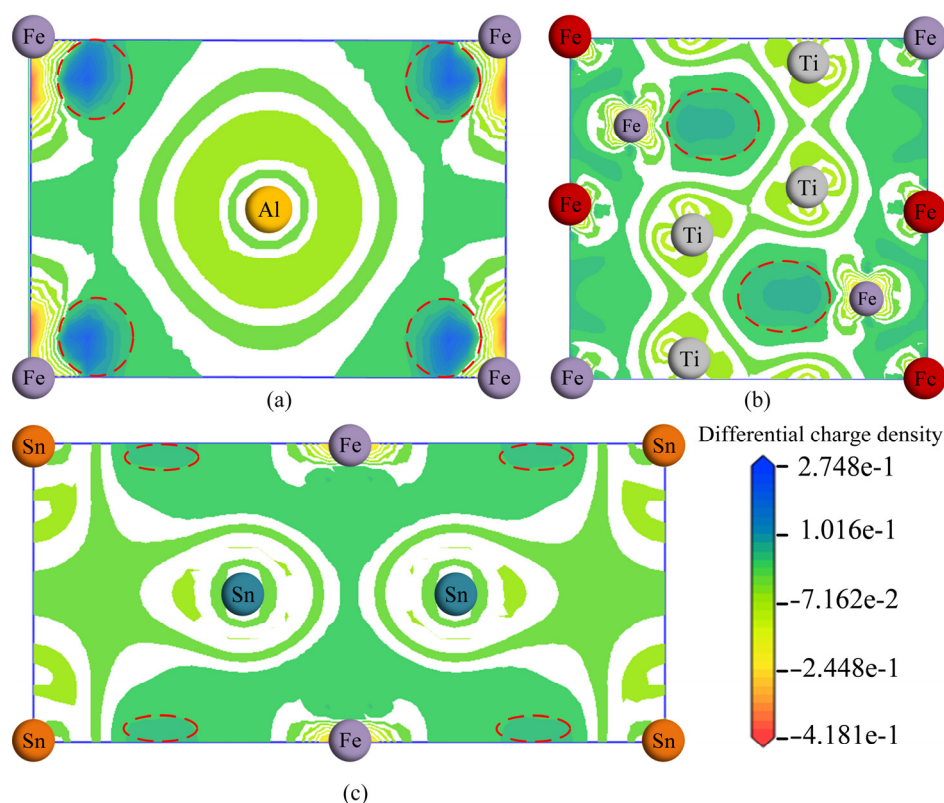


Fig. 5 Differential charge density diagram of FeAl (a), Fe₂Ti (b), and FeSn (c) phases

density diagrams of FeAl, Fe₂Ti and FeSn phases, and the electron density differences of Fe–Al, Fe–Ti and Fe–Sn are marked by the red circle. According to the ruler, the electron density difference of Fe–Al is the biggest, followed by that of Fe–Ti, and that of Fe–Sn is the smallest, which means that the ability of attracting electrons between the above three elements and Fe element is gradually increased in the order of Sn, Ti and Al. Since electronegativity characterizes the ability of an element's atom to attract electrons in compound, the electronegativity difference might cause various charges to transfer between different atoms, leading to the change of electron density difference. Therefore, we speculate that the difference in electron density of Fe–Al, Fe–Ti and Fe–Sn may be caused by the difference in electronegativity of elements of Sn, Ti and Al.

Thirdly, there is a certain correlation between the electron density difference and the bonding effect, and when the electron density difference is small, the bonding effect is weak. Researchers have shown that the less the number of bonding electrons between different atoms is, the less the number of interaction charges within it is, indicating the bonding effect is weak [65]. Thus, from the results

of the total densities of states of FeSn, Fe₂Ti and FeAl phases per atom in Fig. 4(d), the number of bonding electrons in the low-energy state region near the Fermi level E_F of FeSn, Fe₂Ti and FeAl phases can be obtained and the results are shown in Fig. 6. The bonding electron number of FeSn, Fe₂Ti and FeAl is 2.95143, 2.96249 and 3.04471, respectively, which is consistent with the conclusion through comparing the electron density difference.

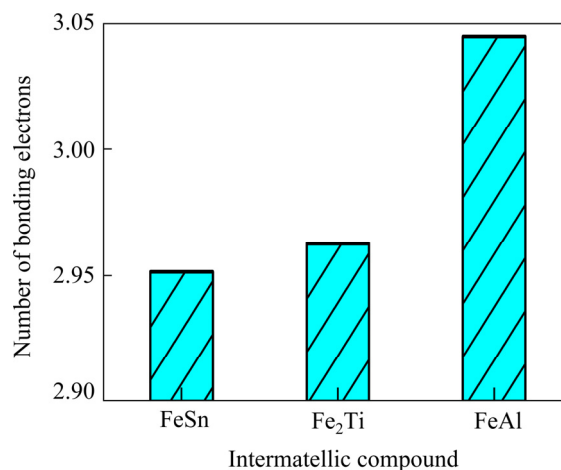


Fig. 6 Number of bonding electrons of FeSn, Fe₂Ti and FeAl near E_F

Based on the above results, we can infer that the transformation mechanism of IMCs formed in steel and aluminum welding from brittle to ductile is due to the weak ability of the interlayer elements to attract electrons, resulting in small electron density difference between Fe and the interlayer elements, which in turn leads to a fewer number of bonding electrons within the IMCs.

3.4 Thermal stability and thermodynamic properties of IMCs

The above elastic constant study indicates that the ductile phase has a strong correlation with the mechanical properties of the joint. However, the above ductile phases' stability is in the ground state, but the temperature variation is very drastic during the process of laser welding. Therefore, it is necessary to investigate the stability of the IMCs at different temperatures. As far as we know, the thermal stability of crystal structure can be investigated from the perspective of thermodynamic features, especially the Gibbs free energy (G'). In order to compare and analyze the structure thermal stability of ductile phases of FeSn, NiAl and Fe₂Ti at different temperatures, thermodynamic properties of entropy, enthalpy and Gibbs free energy of these structures at the elevated temperature were

calculated according to the following standard thermodynamic statistical formulas:

$$G'=H-TS \tag{10}$$

$$H = U + \int c_p dT \tag{11}$$

where H and S are the enthalpy and entropy of the system at different temperatures, respectively; T is the temperature; U is the internal energy; c_p is the specific heat capacity. Thermodynamic properties of these phases are depicted in Fig. 7.

It can be seen from Figs. 7(a) and (b) that the entropy and enthalpy of the three phases increase with the elevated temperature, and the growth rates all gradually increase in the order of FeSn, NiAl and Fe₂Ti. While as presented in Fig. 7(c), the Gibbs free energy of each phase decreases as the temperature increases from 25 to 1000 K. As we all know, the lower the Gibbs free energy of the system is, the higher the thermal stability of the phase structure of the system is. Therefore, the thermal stability of the phases is strengthened with the increase of temperature. Further analysis showed that the Gibbs free energy of the three compounds varies between 200 and 1000 K. Within the temperature range of 200–325 K, the structural stability of FeSn is the highest, followed by NiAl

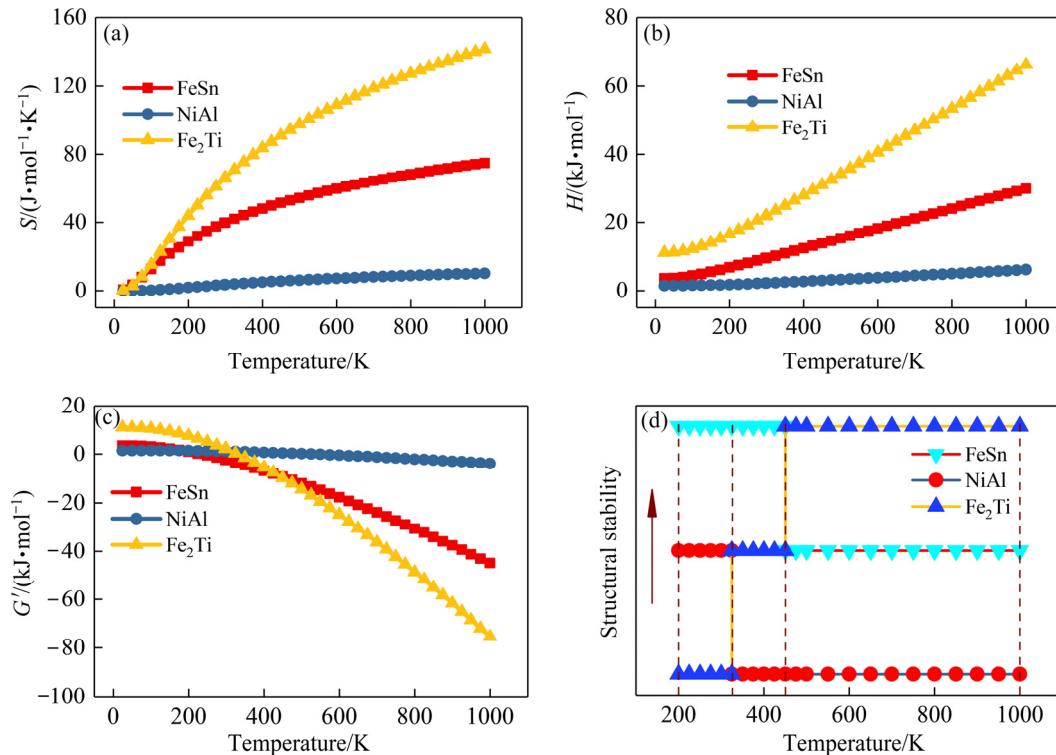


Fig. 7 Entropy (a), enthalpy (b), Gibbs free energy (c), and structural stability (d) of FeSn, NiAl and Fe₂Ti phases at different temperatures

and Fe_2Ti . From 325 to 450 K, the structural stability of FeSn is still the highest, the next are Fe_2Ti and NiAl . While in the range of 450–1000 K, Fe_2Ti becomes the most stable one, followed by FeSn and NiAl . It can be seen that the Gibbs free energy of each phase varies in different temperature ranges.

In terms of selecting alloying element, our main thoughts are as follows: firstly, the alloying ability is assessed by the heat of formation, and the lower the heat of formation is, the stronger the alloying ability is. On this basis, the brittleness/ductility is deduced through the G/B value. According to the first-principles calculation results of the heats of formation of FeSn , NiAl and Fe_2Ti in Table 3, it can be thought that NiAl has the strongest alloying ability, next Fe_2Ti , and finally FeSn , which means that FeSn is relatively difficult to be formed. Further analysis, the heats of formation for NiAl (-69.57 kJ/mol) and Fe_2Ti (-66.48 kJ/mol) are nearly the same. Besides, from the perspective of welding process, the Ti element has the function of improving welding performance of joint and refining grains [66]. Combining with the G/B results of Fe_2Ti and TiAl_3 in Table 4, it is

shown that the element Ti has the effect of reducing brittleness. It is speculated that as an alloying element, Ti can also improve the mechanical properties of steel and aluminum welded joint. Now, the experiments for verification would be introduced in the following text.

4 Results and discussion

According to the above-mentioned theoretical calculation prediction results, we conducted laser welding experiments, SEM, EDS, XRD and shear–tensile tests to verify the effectiveness of the new method using Ti as an alloying element in the steel/aluminum laser welding.

4.1 Interface microstructure and phase composition

The results of EDS point composition analysis and line scanning test are shown in Fig. 8 [67] and Table 5. In general, the formation of IMCs is associated with the elemental content. Therefore, at Points P_1 and P_2 , the Fe/Al molar ratio is very close to 1:1 and 2:5, respectively, which means the IMCs are composed of FeAl and Fe_2Al_5 . The needle-like

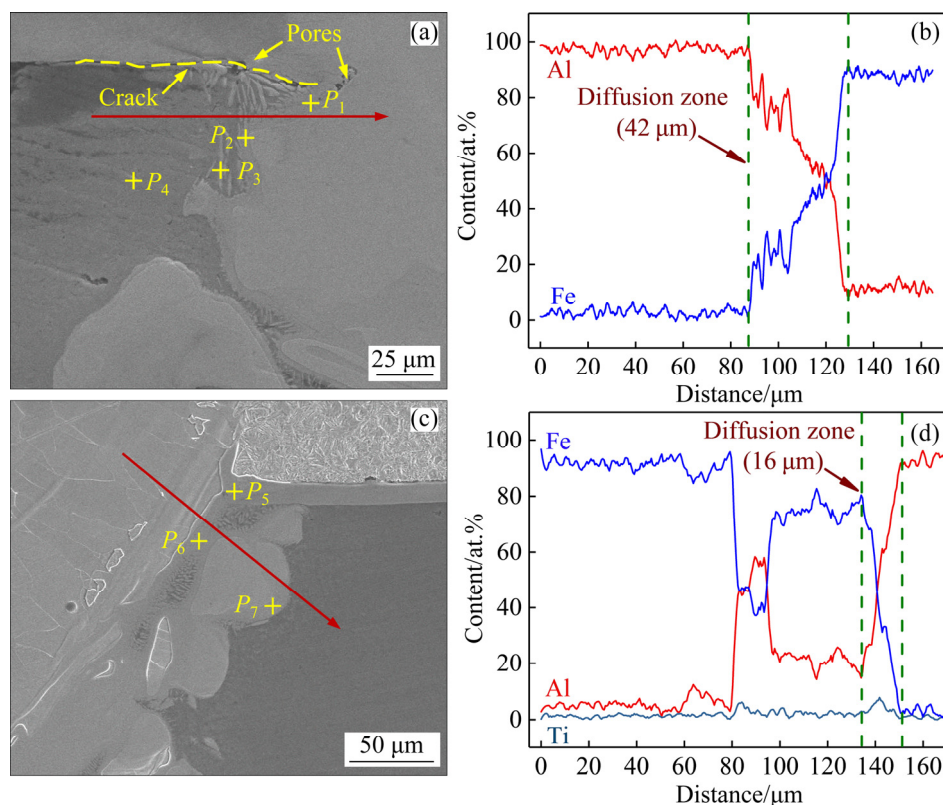


Fig. 8 SEM microstructures of joints: (a) Without Ti foil; (b) Line scanning results in (a); (c) With 0.01 mm-thick Ti foil [67]; (d) Line scanning results in (c) [67]

Table 5 EDS spot composition analysis results in Fig. 8

Point	Content/at.%			Possible phase
	Fe	Al	Ti	
P_1	51.4	48.6	–	FeAl
P_2	27.0	73.0	–	Fe_2Al_5
P_3	14.7	84.63	–	FeAl_3
P_4	0.96	94.93	–	Al
P_5	27.01	2.07	64.36	$\alpha\text{-Ti}+\text{Fe}_2\text{Ti}$
P_6	24.85	70.53	0.27	Fe_2Al_5
P_7	29.0	65.06	4.47	$\text{Fe}_2\text{Al}_5+\text{TiAl}_3$

phase embedded in the Al matrix should be FeAl_3 at P_3 due to the Fe/Al ratio being nearly 1:3. P_4 is identified as Al base metal due to the main Al element. It is worth noting that micro-crack emerges on the layered IMC, which is caused by the brittleness of Fe–Al IMCs. The existence of defects is detrimental to the mechanical properties of the joint.

After adding Ti foil, in Fig. 8(c), P_5 should be composed of $\alpha\text{-Ti}$ and Fe_2Ti according to the results of EDS. As for P_6 , it may be Fe_2Al_5 in view of the Fe/Al ratio being about 2:5. Similarly, P_7 is considered as the mixed phases of Fe_2Al_5 and TiAl_3 formed in the aluminum side molten pool based on the EDS results. According to the results in Figs. 8(b) and (d), the width of the diffusion zone of steel and aluminum decreases from 42 to 16 μm after adding Ti foil, indicating that Ti foil is beneficial to hindering the metallurgical reaction between Fe and Al, reducing the formation of brittle Fe–Al IMCs.

To further confirm the phase compositions before and after adding Ti foil, XRD test was performed and the results are presented in Fig. 9. It can be seen from Fig. 9(a) that FeAl was detected without adding Ti foil. After adding Ti foil, in addition to FeAl and Fe_2Al_5 phases, Fe_2Ti and TiAl_3 new phases were also formed as shown in Fig. 9(b). Thus, the XRD results substantially agree with the above EDS point composition analysis results.

4.2 Mechanical properties and fracture morphologies

For the purpose of analyzing the influence of Ti foil on the mechanical properties of the joint, the shear–tensile test was conducted at room temperature and the results of maximum load are exhibited in Fig. 10. Compared with the maximum

load of 1272 N without adding Ti foil, the maximum load increases to 1406 N when the Ti foil thickness is 0.01 mm, which means that the mechanical properties of the joint are improved by about 11%. Therefore, adding the alloying element Ti for metallurgical regulation could effectively enhance the mechanical properties of steel and aluminum welding joint.

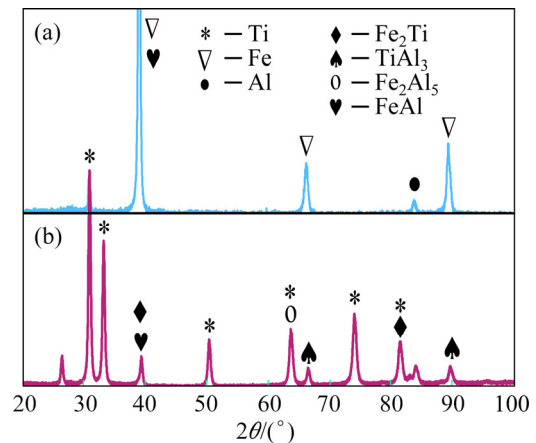


Fig. 9 XRD patterns of joints: (a) Without Ti foil; (b) With 0.01 mm-thick Ti foil

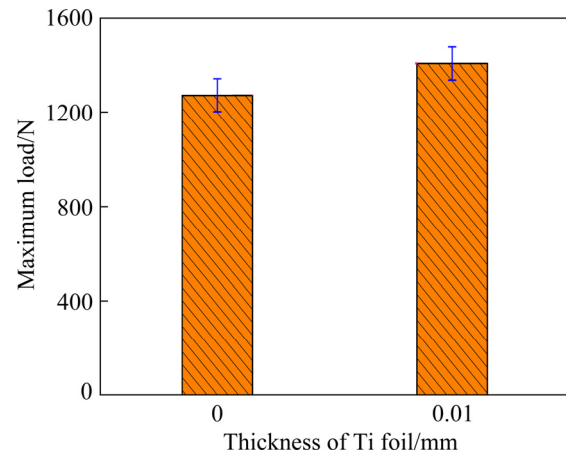


Fig. 10 Maximum load comparison of joint with or without Ti foil

Figure 11 exhibits the fracture morphologies of the joints after shear–tensile test. From Fig. 11(a), there is a river-like pattern of cleavage platform on the fracture surface, which is a typical characteristic of brittle fracture, indicating that the fracture mode of the joint is brittle fracture when no Ti foil is added. According to the EDS spot scanning results in Table 6, the phases at Point A, B and C are Fe_2Al_5 due to the Fe/Al ratio being nearly 1:3, indicating that the fracture of the joint is caused by the brittle Fe_2Al_5 phase. In Fig. 11(b), there are not only

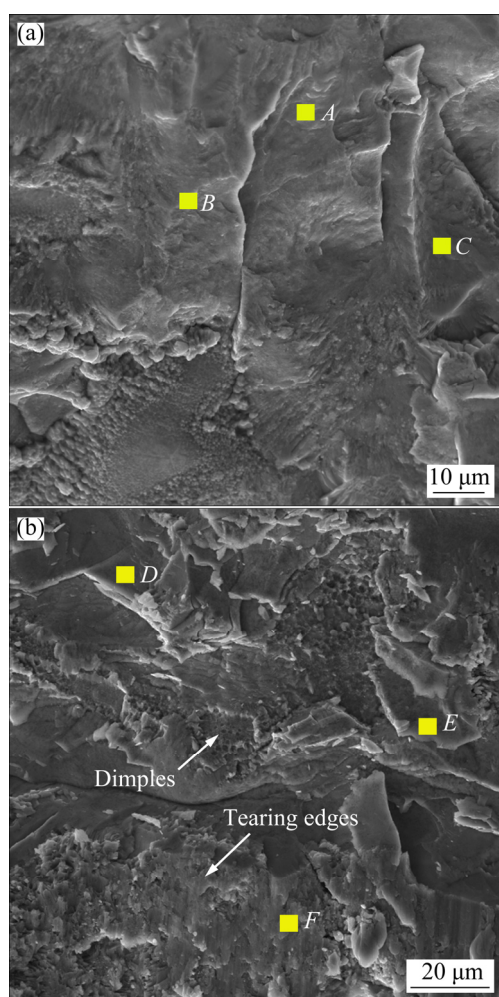


Fig. 11 SEM images of fracture position and fracture morphology of joints without or with Ti foil: (a) Without Ti foil; (b) With 0.01 mm-thick Ti foil

Table 6 EDS spot composition analysis results in Fig. 11

Point	Content/at.%			Possible phase
	Fe	Al	Ti	
A	26.86	73.14	–	Fe ₂ Al ₅
B	30.35	69.65	–	Fe ₂ Al ₅
C	29.55	70.45	–	Fe ₂ Al ₅
D	30.45	69.18	0.37	Fe ₂ Al ₅
E	27.95	71.7	0.35	Fe ₂ Al ₅
F	92.58	7.11	0.31	Al

cleavage plane patterns, but also some obvious dimples and tearing edges, which means that the fracture mode changes into a mixture of brittle and ductile fractures after adding Ti foil. Similarly, the phases at Point D and E are also Fe₂Al₅ according to the ratio of Fe and Al. Additionally, the phase at Point F is Al matrix, which means that part of the

fractures occur in the Al base metal.

The above results indicate that the fracture is caused by Fe₂Al₅ brittle phase whether the Ti foil is added. This is because Fe₂Al₅ has the highest brittleness and hardness, which is prone to induce crack when the joint is under load. Similar result has been confirmed by INDHU et al [68]. After adding Ti foil, the fracture surface has part of Al matrix, indicating that part of fractures locate at the Al base metal, which means that the toughness of the joint is enhanced. Since the ductile Fe₂Ti and low-brittleness TiAl₃ phases have not been detected on the fracture surface, we can conclude that the improvement of the mechanical properties of the joint after adding Ti foil is achieved by reducing the brittleness of the joint. The above experimental results well confirm the first-principles calculation prediction in Section 3.

5 Conclusions

(1) The generated IMCs caused by adding interlayer are of sound alloying ability as well as good structural stability. Brittleness of the Fe–Al IMCs is attributed to the orbital hybridization between Al(s), Al(p) and Fe(d), and ductility of the generated IMCs benefits from the changes of electronic structure. Due to the weak ability of interlayer elements to attract electrons, the differences in charge density between Fe and interlayer elements are smaller than that of Fe and Al elements, resulting in the number of bonding electrons of the generated IMCs being less than that of Fe–Al IMCs.

(2) The mechanical properties of the steel/aluminum joint are limited by the brittle Fe–Al IMCs. However, the joint properties are improved by adding interlayer with the IMCs changed from brittle to ductile. The mechanical properties of the joint are closely related to the ductility or brittleness of the IMCs.

(3) According to the *G/B* results of Fe₂Ti and TiAl₃, it is speculated that Ti as alloying element can improve the mechanical properties of steel–aluminum welded joint. The experimental verification is in good agreement with the theoretical calculation prediction.

Acknowledgments

The authors are grateful for the financial

supports from the National Natural Science Foundation of China (Nos. 51674112, 51774125).

References

- [1] DILTHEY U, STEIN L. Multimaterial car body design: Challenge for welding and joining [J]. *Science and Technology of Welding and Joining*, 2006, 11(2): 135–142.
- [2] ZHOU He, LIU Jin-shui, ZHOU Dian-wu, TAO Tao. Effect of Al-foil addition on microstructure and temperature field of laser fusion welded joints of DP590 dual-phase steel and AZ31B magnesium alloy [J]. *Transactions of Nonferrous Metals Society of China*, 2020, 30(10): 2669–2680.
- [3] CHENG Bo, WU Dong-jiang, ZHANG Chao, CHAI Dong-sheng, MA Guang-yi. Transformation mechanism of secondary phase and its effect on intergranular corrosion in laser wire filling welding Ni-based alloy/304 stainless steel [J]. *Transactions of Nonferrous Metals Society of China*, 2021, 31(3): 715–725.
- [4] PERVAIZ M, PANTHAPULAKKAL S, KC B, SAIN M, TJONG J. Emerging Trends in Automotive Lightweighting through Novel Composite Materials [J]. *Materials Sciences and Applications*, 2016, 7(1): 26–38.
- [5] PUGH S F. XCII. Relations between the elastic moduli and the plastic properties of polycrystalline pure metals [J]. *The London, Edinburgh, and Dublin Philosophical Magazine and Journal of Science*, 2009, 45(367): 823–843.
- [6] GANESHAN S, SHANG S L, WANG Y, LIU Z K. Effect of alloying elements on the elastic properties of Mg from first-principles calculations [J]. *Acta Materialia*, 2009, 57(13): 3876–3884.
- [7] SHINODA W, SHIGA M, MIKAMI M. Rapid estimation of elastic constants by molecular dynamics simulation under constant stress [J]. *Physical Review B*, 2004, 69(13): 134103.
- [8] SUMER A, SMITH J F. Elastic constants of single-crystal CaMg_2 [J]. *Journal of Applied Physics*, 1962, 33(7): 2283–2286.
- [9] MATTESINI M, AHUJA R, JOHANSSON B. Cubic Hf_3N_4 and Zr_3N_4 : A class of hard materials [J]. *Physical Review B*, 2003, 68(18): 184108.
- [10] GSCHNEIDNER K J, RUSSELL A, PECHARSKY A, MORRIS J, ZHANG Zhe-hua, LOGRASSO T, HSU D, CHESTER LO C H, YE Yi-ying, SLAGER A, KESSE D. A family of ductile intermetallic compounds [J]. *Nature Materials*, 2003, 2(9): 587–591.
- [11] TVERGAARD V, HUTCHINSON J W. Microcracking in ceramics induced by thermal expansion or elastic anisotropy [J]. *Journal of the American Ceramic Society*, 1988, 71(3): 157–166.
- [12] LIU A Y, COHEN M L. Prediction of new low compressibility solids [J]. *Science*, 1989, 245(4920): 841–842.
- [13] LIU Xiu-bo, YU Gang, GUO Jian, GU Yi-jie, PANG Ming, ZHENG Cai-yun, WANG Heng-hai. Research on laser welding of cast Ni-based superalloy K418 turbo disk and alloy steel 42CrMo shaft [J]. *Journal of Alloys and Compounds*, 2008, 453(1–2): 371–378.
- [14] CHEN Shu-hai, HUANG Ji-hua, MA Ke, ZHAO Xing-ke, VIVEK A. Microstructures and mechanical properties of laser penetration welding joint with/without Ni-foil in an overlap steel-on-aluminum configuration [J]. *Metallurgical and Materials Transactions A*, 2014, 45(7): 3064–3073.
- [15] ZHOU Dian-wu, PENG Yan, XU Shao-hua, LIU Jin-shui. Microstructure and mechanical property of steel/Al alloy laser welding with Sn powder addition [J]. *Acta Metallurgica Sinica*, 2013, 49(8): 959: 959–968.
- [16] ZHOU Dian-wu, XU Shao-hua, ZHANG Li-juan, PENG Yan, LIU Jin-shui. Microstructure, mechanical properties, and electronic simulations of steel/aluminum alloy joint during deep penetration laser welding [J]. *The International Journal of Advanced Manufacturing Technology*, 2016, 89(1–4): 377–387.
- [17] ZHOU Dian-wu, TIAN Wei, PENG Li, ZHANG Yi, CHEN Gen-yu. Laser lap welding of steel and aluminum alloy with Cu, Pb metal sandwich addition [J]. *Rare Metal Materials and Engineering*, 2014, 43(5): 1181–1186.
- [18] PENG Yan, ZHOU Dian-wu, XU Shao-hua, PENG Ping, LIU Jin-shui. First-principles studies of the effects of microalloy elements on Fe/Al interface for laser lap welding of steel and aluminum [J]. *Rare Metal Materials and Engineering*, 2012, 41: 302–306.
- [19] ZHOU Dian-wu, LIU Jin-shui, LU Yuan-zhi, XU Shao-hua. Effect of adding powder on joint properties of laser penetration welding for dual phase steel and aluminum alloy [J]. *Optics & Laser Technology*, 2017, 94: 171–179.
- [20] PAYNE M C, TETER M P, ALLAN D C, ARIAS T. Iterative minimization techniques for ab initio total-energy calculations: Molecular dynamics and conjugate gradients [J]. *Reviews of Modern Physics*, 1992, 64(4): 1045–1097.
- [21] WHITE J, BIRD D. Implementation of gradient-corrected exchange-correlation potentials in Car–Parrinello total-energy calculations [J]. *Physical Review B*, 1994, 50(7): 4954–4957.
- [22] PERDEW J P, CHEVARY J A, VOSKO S H, JACKSON K A, PEDERSON M R, SINGH D J, FIOHLAIS C. Atoms, molecules, solids, and surfaces: Applications of the generalized gradient approximation for exchange and correlation [J]. *Physical Review B*, 1992, 46(11): 6671–6687.
- [23] MONKHORST H J, PACK J D. Special points for Brillouin-zone integrations [J]. *Physical Review B*, 1976, 13(12): 5188–5192.
- [24] VANDERBILT D. Soft self-consistent pseudopotentials in a generalized eigenvalue formalism [J]. *Physical Review B*, 1990, 41(11): 7892–7895.
- [25] LOO F J J V, RIECK G D. Diffusion in the titanium–aluminium system—I. Interdiffusion between solid Al and Ti or Ti–Al alloys [J]. *Acta Metallurgica*, 1973, 21(1): 61–71.
- [26] WANG S Q, PATEL V K, BHOLE S D, WEN G D, CHEN D L. Microstructure and mechanical properties of ultrasonic spot welded Al/Ti alloy joints [J]. *Materials & Design*, 2015, 78: 33–41.
- [27] CHU Qiao-ling, ZHANG Min, LI Ji-hong, YAN Cheng, QIN Zhan-ling. Influence of vanadium filler on the properties of titanium and steel TIG welded joints [J]. *Journal of Materials Processing Technology*, 2017, 240: 293–304.

- [28] SHAOJUN L, SUQING D, BENKUN M. First-principles calculation of vibrational entropy for Fe–Al compounds [J]. *Physical Review B*, 1998, 58(58): 9705–9709.
- [29] LEE E, LEE B J. Modified embedded-atom method interatomic potential for the Fe–Al system [J]. *Journal of Physics Condensed Matter: An Institute of Physics Journal*, 2010, 22(17): 175702.
- [30] CONNÉTABLE D, MAUGIS P. First principle calculations of the κ -Fe₃AlC perovskite and iron–aluminium intermetallics [J]. *Intermetallics*, 2008, 16(3): 345–352.
- [31] ZHANG Chan-hui, HUANG Shuo, SHEN Jiang, CHEN Nan-xian. Structural and mechanical properties of Fe–Al compounds: An atomistic study by EAM simulation [J]. *Intermetallics*, 2014, 52: 86–91.
- [32] SINGH D J. Electronic structure, magnetism, and stability of Co-doped NiAl [J]. *Physical Review B*, 1992, 46(22): 14392–14397.
- [33] HUANG X, NAUMOV I I, RABE K M. Phonon anomalies and elastic constants of cubic NiAl from first principles [J]. *Physical Review B*, 2004, 70(6): 064301.
- [34] YAN Xin-lin, CHEN Xing-qiu, GRYTSIV A, WITUSIEWICZ V T. Site preference, thermodynamic, and magnetic properties of the ternary Laves phase Ti(Fe_{1-x}Al_x)₂ with the crystal structure of the MgZn₂-type [J]. *Zeitschrift für Metallkunde*, 2006, 97(4): 450–460.
- [35] CHEN Zhen-lian, ZOU Hua-min, YU Feng-mei, ZOU Jie. Chemical bonding and pseudogap formation in D022- and L12-structure (V,Ti)Al₃ [J]. *Journal of Physics and Chemistry of Solids*, 2010, 71(7): 946–951.
- [36] FU C L. Electronic, elastic, and fracture properties of trialuminide alloys: Al₃Sc and Al₃Ti [J]. *Journal of Materials Research*, 1990, 5(5): 971–979.
- [37] SIMMONS G, WANG H. Single crystal elastic constants and calculated aggregate properties: A handbook [M]. Cambridge: MIT Press, 1971: 34–60.
- [38] TURCHI P, REINHARD L, STOCKS G. First-principles study of stability and local order in bcc-based Fe–Cr and Fe–V alloys [J]. *Physical Review B*, 1994, 50(21): 15542–15558.
- [39] WALLACE D C. Thermodynamics of crystals [J]. *American Journal of Physics*, 1972, 40(11): 1718–1719.
- [40] OHBA T, KITANO Y, KOMURA Y. The charge-density study of the Laves phases, MgZn₂ and MgCu₂ [J]. *Acta Crystallographica*, 1984, 40(1): 1–5.
- [41] VILLARS P, CALVERT L D, PEARSON W B. Pearson's handbook of crystallographic data for intermediate phases [J]. *Acta Crystallographica*, 1985, 40(1): C444.
- [42] DUTCHAK Y I, CHEKH V G. High temperature X-ray diffraction study of the lattice dynamics of the compounds AlCo and AlNi [J]. *Zhurnal Prikladnoi Khimii*, 1981, 55: 2342–2345.
- [43] MEDVEDEVA N I, GORNOSTYREV Y N, NOVIKOV D L, MRYASOV O N, FREEMAN A J. Ternary site preference energies, size misfits and solid solution hardening in NiAl and FeAl [J]. *Acta Materialia*, 1998, 46(10): 3433–3442.
- [44] KANG S J, PARK S, KIM M, HAN H N, LEE S K, LEE K Y, KWON Y K. Enhanced mechanical property of Fe–Al alloy due to Mn insertion: ab initio study [J]. *Journal of Alloys and Compounds*, 2014, 583: 295–299.
- [45] CAO Yong, ZHU Pei-xian, ZHU Jing-chuan, LIU Yong. First-principles study of NiAl alloyed with Co [J]. *Computational Materials Science*, 2016, 111: 34–40.
- [46] ASTA M, FONTAINE D D, SCHILFGAARDE M V, SLUITER M, METHESSE M. First-principles phase-stability study of fcc alloys in the Ti–Al system [J]. *Physical Review B*, 1992, 46(9): 5055–5072.
- [47] HONG T, WATSON-YANG T J, FREEMAN A J, OUGCHI T, XU J H. Crystal structure, phase stability, and electronic structure of Ti–Al intermetallics: TiAl₃ [J]. *Physical Review B*, 1990, 41(18): 12462–12467.
- [48] DESAI P D. Thermodynamic properties of selected binary aluminum alloy systems [J]. *Journal of physical and chemical reference data*, 1987, 16(1): 109–124.
- [49] GONZALES-ORMEÑO P G, PETRILLI H M, SCHÖN C G. Ab-initio calculations of the formation energies of BCC-based superlattices in the Fe–Al system [J]. *Calphad*, 2002, 26(4): 573–582.
- [50] DELSANTE S, GHOSH G, BORZONE G. A calorimetric study of alloys along the Ti(Zn,Al)₃ section [J]. *Calphad*, 2009, 33(1): 50–54.
- [51] MESCHEL S, KLEPPA O. The standard enthalpies of formation of some 3d transition metal aluminides by high-temperature direct synthesis calorimetry [M]. Berlin: Springer, 1994: 103–112.
- [52] NASSIK M, CHRIFI-ALAOUI F Z, MAHDOUK K, GACHON J C. Calorimetric study of the aluminum–titanium system [J]. *Journal of Alloys and Compounds*, 2003, 350: 151–154.
- [53] KUBASCHEWSKI O, HEYMER G. Heats of formation of transition-metal aluminides [J]. *Transactions of the Faraday Society*, 1960, 56: 473–478.
- [54] KUBASCHEWSKI O, DENCH W. The heats of formation in the systems titanium–aluminium and titanium–iron [J]. *Acta Metall*, 1955, 3(4): 339–346.
- [55] RAVINDRAN P, FAST L, KORZHAVYI P A, JOHANSSON B, WILLS J, ERIKSSON O. Density functional theory for calculation of elastic properties of orthorhombic crystals: Application to TiSi₂ [J]. *Journal of Applied Physics*, 1998, 84(9): 4891–4904.
- [56] MOUHAT F, COUDERT F X. Necessary and sufficient elastic stability conditions in various crystal systems [J]. *Physical Review B*, 2014, 90(22): 224104.
- [57] VAILHE C, FARKAS D. Shear faults and dislocation core structure simulations in B2 FeAl [J]. *Acta Materialia*, 1997, 45(11): 4463–4473.
- [58] WANG Y, LIU Z K, CHEN L Q. Thermodynamic properties of Al, Ni, NiAl, and Ni₃Al from first-principles calculations [J]. *Acta Materialia*, 2004, 52(9): 2665–2671.
- [59] DAVENPORT T, ZHOU L, TRIVISONNO J. Ultrasonic and atomic force studies of the martensitic transformation induced by temperature and uniaxial stress in NiAl alloys [J]. *Physical Review B*, 1999, 59(5): 3421–3426.
- [60] NAKAMURA M, KIMURA K. Elastic constants of TiAl₃

- and $ZrAl_3$ single crystals [J]. Journal of materials science, 1991, 26(8): 2208–2214.
- [61] MEHL M J, OSBURN J E, PAPACONSTANTOPOULOS D A, KLEIN B M. Structural properties of ordered high-melting-temperature intermetallic alloys from first-principles total-energy calculations [J]. Physical Review B, 1990, 41(15): 10311–10323.
- [62] HONG S, FU C L. Phase stability and elastic moduli of Cr_2Nb by first-principles calculations [J]. Intermetallics, 1999, 7(1): 5–9.
- [63] TSE J S. Intrinsic hardness of crystalline solids [J]. Journal of Superhard Materials, 2010, 32(3): 177–191.
- [64] CHEN Xing-qiu, NIU Hai-yang, LI Dian-zhong, LI Yi-yi. Modeling hardness of polycrystalline materials and bulk metallic glasses [J]. Intermetallics, 2011, 19(9): 1275–1281.
- [65] FU C L, WANG X D, YE Y Y, HO K M. Phase stability, bonding mechanism, and elastic constants of Mo_5Si_3 by first-principles calculation [J]. Intermetallics, 1999, 7(2): 179–184.
- [66] TROIANO, ALEXANDER R. The role of hydrogen and other interstitials in the mechanical behavior of metals [J]. Metallography Microstructure & Analysis, 2016, 5(6): 557–569.
- [67] LI Tian, ZHOU Dian-wu, YAN You-ruì-ling, ZHANG Shu-mai, LIU Jin-shui. Effect of Ti foil on microstructure and mechanical properties of laser fusion welding of DP590 dual-phase steel to 6022 aluminum alloy [J]. Materials Science and Engineering A, 2020: 139929.
- [68] INDHU R, SOUNDARAPANDIAN S, VIJAYARAGHAVAN L. Yb: YAG laser welding of dual phase steel to aluminum alloy [J]. Journal of Materials Processing Technology, 2018, 262: 411–421.

钢/铝激光焊接接头性能与金属间化合物延/脆性的第一性原理和实验研究

李 田¹, 周愫武¹, 严佑锐凌¹, 彭 平², 刘金水²

1. 湖南大学 汽车车身先进设计制造国家重点实验室, 长沙 410082;
2. 湖南大学 材料科学与工程学院, 长沙 410082

摘 要: 采用扫描电子显微镜、能谱仪、X 射线衍射仪以及第一性原理计算方法, 研究钢/铝激光焊接形成的金属间化合物(IMCs)的形貌、分布、相组成、形成能力、结构稳定性和本征力学性质。结果发现, 脆性 Fe–Al 化合物限制钢/铝接头力学性能, 其脆性电子结构根源在于 Al(s)、Al(p)和 Fe(d)之间的轨道杂化; 添加中间夹层可改善钢/铝接头的力学性能, 归因于形成的金属间化合物电子结构的改变; 金属间化合物由脆性向延性的转变机制主要归因于夹层元素吸引电子的能力弱。钢/铝焊接头的力学性能与金属间化合物的延/脆性密切相关, 添加 Ti 箔有效提高接头的力学性能, 表明实验验证与理论计算预测吻合较好。

关键词: 第一性原理计算; 弹性常数; 延性; 脆性; 激光焊接; 力学性能

(Edited by Wei-ping CHEN)